POLITECNICO DI TORINO
Repository ISTITUZIONALE

TeraHertz Vibrations and Phono-Fission Reactions from Crushing of Iron-rich Natural Rocks

(Article begins on next page)
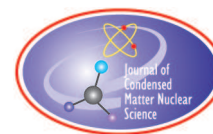
15 May 2024

TeraHertz Vibrations and Phono-Fission Reactions from Crushing of Iron-rich Natural Rocks

Alberto Carpinteri* and Oscar Borla

Department of Structural, Geotechnical and Building Engineering, Politecnico di Torino, Corso Duca degli Abruzzi 24, 10129 Torino, Italy

Umberto Lucia and Massimo Zucchetti

Dipartimento Energia "Galileo Ferraris", Politecnico di Torino, Corso Duca degli Abruzzi 24, 10129 Torino, Italy

Abstract

Brittle crushing of iron-rich natural rocks was demonstrated to produce neutron emission, sometimes orders of magnitude larger than the environmental background. Chemical composition changes and a global ponderal equivalence, respecting atomic weight and atomic number balances, were observed. Phonons and plasmons induced by brittle crushing, if sufficiently energetic and resonant with the atomic lattice, may split the nucleus into different fragments and neutrons. It is relevant to emphasize how the earth's crust evolution from basaltic to sialic can be consistently explained by these experimental data and theoretical assumptions when applied to tectonics.

Keywords: Natural rock crushing, nuclear reactions, phonons, plasmons, spalling neutrons, resonance

1. Introduction

Recently, a new explanation of the neutron emissions from stone breaking has been suggested [1], i.e., the phono-fission reactions repeatedly revealed in a great number of experiments [2]–[5]. The approach was based on the spalling effects generated by the plasmon-lattice interaction [1]. Indeed, different types of detectors have demonstrated the presence of neutron emissions, in some cases by several orders of magnitude higher than the usual environmental background [2]–[5]. Any solid body is subjected to rapid fluctuations for a few moments when it breaks in a brittle way, even if only partially, or when the formation and propagation of micro-cracks occurs. Macroscopically, this appears in the form of longitudinal waves of expansion-contraction (tension-compression), in addition to transverse (shear) waves [2]–[5]. Microscopically, these pressure waves are phonons or plasmons in relation to the frequency under consideration [6]–[9]. Even if phonons and plasmons originate from different mechanisms, they are both bosons in the many-body quasi-particle perspective, and share several similarities. In particular, a plasma oscillation can

---

*Corresponding author: alberto.carpinteri@polito.it

be considered as a sort of longitudinal phonon in which the elastic modulus, as well as the frequency of transverse oscillation, is equal to zero [8].

At the nanoscale, the frequency measured is that at the order of terahertz [2]–[5], [10], [11]. During the experimental activities, significant neutron emissions (phono-fission neutrons) have been repeatedly measured [2]–[5], [10]. The neutron flux was found to depend on the iron content, and besides this, on the size of the specimen, through the well-known brittleness size effect [11]. Larger sizes imply a higher brittleness, i.e. a more relevant strain energy emission, and therefore more neutrons.

Moreover, the resulting nuclear transmutations are particularly evident for loadstones, which leads to the conclusion that they happen as a consequence of photo-disintegration [12]–[15]. The electro-strong coupling between electromagnetic fields and nuclear giant dipole resonances has been considered as the theoretical core for the explanation of the observed nuclear reactions. The electro-weak interactions can produce neutrons from energetic protons and electrons, thus inducing nuclear transmutations. The electro-strong condensed matter coupling can represent many new body collective nuclear photo-disintegration effects [12], [16]–[18]. On the other hand, the spalling neutrons approach is very useful in explaining the experimental results obtained in relation to the neutron emissions from stone breaking. Moreover, it allows us also to link the experimental results to the energy-mass conversion balance inside solid lattices. Indeed, it recalls some new discussions on mass [19] in the universe, founded on the fundamental laws of physics, with particular regards to the principle of least action [19]–[22]. In this context, the discrete character of nature was proven to be reflected in multiplicity at all levels of its hierarchical organization [19]–[22], and that the basic geometry implies also how baryons could pack together in an atomic nucleus. In this way, it has been highlighted how a coordinate of space embodies a closed circulation of energy, and a moment of time will elapse when the circulation opens up either to acquire or discard quantized flux of energy [23]. Consequently, the mass of a body depends on how much its energy density on the least-action path perturbs, i.e. the elastic energy of the solid lattice. Therefore, the curvature and chirality of particular paths invariably relate gravitational and electromagnetic interactions, as well as weak and strong interactions, with one another [19].

These last considerations allow us to introduce further ones on the links among solid lattice and the fundamental interactions inside the solids.

The key mechanisms through which low-energy nuclear reactions can occur are well known: for neutron production (and subsequent nuclear transmutations) via weak interactions, special conditions in condensed matter systems must be found, which accelerate an electron to MeV range of energies. If certain particular conditions are verified, the electromagnetic energy stored in many relatively slow-moving electrons can be collectively transferred into fewer, much faster electrons with energies sufficient for the latter to combine with protons (or deuterons, if present) to produce neutrons via weak interactions. In this way, electromagnetic and weak interactions can induce low-energy nuclear reactions to occur with observable rates for a variety of processes. The produced neutrons can then initiate low-energy nuclear reactions through further nuclear transmutations.

In this paper, a novel tentative explanation of some experimental results will be given by means of a theory starting from collective oscillations of electronic density inside the solid lattice, i.e., plasmons.

2. Materials and Methods

A plasmon is a collective oscillation of the electronic density [7]–[9] inside the solid lattice. At the equilibrium state, the electric charge of the electronic gas is balanced by the electric charge of the nuclei of the lattice knots [7]–[9], whereas, when the electron gas moves through a lattice dislocation, a charge asymmetry occurs on the opposite sides of the dislocation itself with the consequent generation of a reactive force which causes a simple harmonic motion at

the plasmonic frequency [6]:

$$\omega_{ph}^2 = \frac{ne^2}{\varepsilon_0 m_{eff}} \tag{1}$$

where n is the electron density, e is the electric charge of the electron, ε_0 is the electric permittivity in vacuum, and m_{eff} is the effective electron mass. For the crushing of iron-rich natural rocks, the plasmonic frequency has been obtained [1] as (see Appendix):

$$\omega_{ph}^2 = \frac{n_{eff}e^2}{\varepsilon_0 m_{eff}} = \frac{2\pi c^2}{a^2 \ln\left(\frac{a}{r}\right)} \tag{2}$$

with:

$$n_{eff} = \frac{A}{a^2}n \tag{3}$$

where a is the lattice constant, c is the speed of light and n_{eff} is the number of electrons which concur to the plasmonic frequency. This number is not equal to the total number of all electrons, but only to the ones really in motion inside the dislocation, in a direction perpendicular to the dislocation surface itself, of area $A = \pi r^2$. The electronic motion generates a magnetic field, which produces a self-induction effect with a consequent superposition of different forces acting on the electrons: the resulting effect is represented by the apparent effective mass of the electrons [6]:

$$m_{eff} = \frac{\mu_0}{2\pi} ne^2 A \ln\left(\frac{a}{r}\right) \tag{4}$$

where μ_0 is the magnetic permeability in vacuum, introduced in relation to the self-inductance of the current generated by the electron motion in accordance with [6], and r is the radius of the virtual cylinder generated by the electron trajectories. Plasmons produce important effects on the physical properties of matter interacting with electromagnetic fields, because they generate a relative electric permittivity:

$$\varepsilon(\omega) = 1 - \frac{\omega_{ph}^2}{\omega\,(\omega + i\gamma)} \tag{5}$$

where γ is the damping factor and ω is the electromagnetic frequency. The value of relation (5) is negative for frequencies lower than the plasmonic ones. The physical meaning of this negative electric permittivity consists in the generation of electromagnetic structures at the border of dislocations.

It was also highlighted how the scattering of the electronic motion inside the dislocation presents the same inertial effect as that of a nucleus of the same velocity [1].

In addition, the usual values of the damping factor and of the plasma frequency for iron (as well as for other metals) are in the terahertz band [23], [24]. Thus, during the crushing of the iron-rich rocks, a resonant scattering of plasmons occurs with a characteristic frequency of the latter around 1 TeraHertz. Therefore, the plasmons are absorbed by the lattice nuclei with the following nuclear reaction:

$$^A_Z X + \gamma_{ph} \rightarrow {}^A_Z X^* \rightarrow {}^{A_1}_{Z_1} X + {}^{A_2}_{Z_2} X + Nn \tag{6}$$

where X is the lattice nucleus, A is its mass number, Z is its atomic number, n is the spalling neutron, N its number, γ_{ph} is the incoming plasmon [7]–[9], [25], [26] and X* is the compound nucleus X. Reaction (6) is no more than a resonant effect related to the absorption of the phonon; consequently, the extraction energy for the neutrons, related to reaction (6), can be evaluated as follows [25]:

$$E_{em,Nn} = 931 \cdot [M(Z_1, A_1) + M(Z_2, A_2) + m_{ph} - N\,m_n - M(Z, A) + (Z - Z_1 - Z_2)\,m_e] \tag{7}$$

and the energy of any neutron can be evaluated as [25]:

$$E_{k,n} = \frac{1}{N} \frac{A-N}{A} \left(E_{ph} - E_{em,Nn} \right). \tag{8}$$

3. Results and Discussions

In order to discuss the previous results, we must consider some possible reactions [2]–[5] for Fe, as for example:

$$^{56}_{26}\text{Fe} \rightarrow 2\, ^{27}_{13}\text{Al} + 2\text{n} \tag{9}$$

$$^{56}_{26}\text{Fe} \rightarrow\, ^{24}_{12}\text{Mg} +\, ^{28}_{14}\text{Si} + 4\text{n} \tag{10}$$

where the spalled neutrons (with a resultant energy in the GeV order of magnitude) are expelled together with two main fragments of the nucleus. In addition, the plasmons in the lattice under crushing have an effective mass (m_{eff}) between 5 and 7 times the proton mass (m_p) and a frequency in the terahertz band. In the following, the frequency and the effective mass of the plasmons for the different minerals characterizing the rocks tested during the several experimental campaigns are reported: Phengite, $\omega_{ph} = 16.1$ TeraHertz and $m_{eff} = 6.9\, m_p$; Biotite, $\omega_{ph} = 15.4$ TeraHertz and $m_{eff} = 7.1\, m_p$; Olivine, $\omega_{ph} = 24.6$ TeraHertz and $m_{eff} = 5.2\, m_p$; Magnetite, $\omega_{ph} = 17.8$ TeraHertz and $m_{eff} = 6.5\, m_p$.

On the other hand, the neutron emissions experimentally monitored by means of He^3 proportional counter, and summarized in the next section, refer to the low energy component. As a matter of fact, the elastic and inelastic interactions of neutrons with matter contribute to the energy slowing down reaching values typical of the thermal component (0.025 eV).

We must highlight that the reactions (9) and (10) are the consequence of the absorbed plasmon, and this absorption can be linked to a resonance phenomenon. Consequently, the nucleus jumps to an excited state, and after a time of $10^{-14} - 10^{-13}$ s the reaction occurs.

4. Experimental Results

The theoretical results obtained in the previous sections must be experimentally confirmed. To do so, we consider some experiments recently published, just to be sure of the results. Neutron emissions were measured during laboratory experiments conducted on iron-rich rocks. In particular, magnetite specimens were loaded up to the final failure under monotonic displacement control. Also basalt rocks were tested under cyclic loading conditions (2 Hz) up to the final failure. In order to detect neutron emissions, the tests were monitored by two different neutron measurement devices: He3 proportional counter and thermodynamic (bubble) detectors. After the experiments, Energy Dispersive X-Ray Spectroscopy (EDS) analyses were carried out to detect possible direct evidence of low energy nuclear reactions on the fracture surfaces. In particular, quantitative evidence of nuclear reactions, involving iron decrease and the corresponding increase in lighter elements, were observed in the olivine, crystalline mineral phase widely diffused in the basalt matrix, and in the magnetite. These results reinforce the evidences previously observed for Luserna stone (granitic orthogneiss) and confirm that phono-fissions take place in natural iron-bearing materials subjected to damage accumulation and cracking.

4.1. Granite

Preliminary tests on prismatic specimens were presented in previous contributions, recently published [4], [27], [28], and related to phono-fission reactions occurring in solids containing iron (samples of Luserna stone in compression). In a preliminary experiment, four specimens were tested, two made of Carrara Marble and two made of Luserna stone

[4], [27], [28]. All of them were of the same size and shape, measuring $6 \times 6 \times 10$ cm^3. The neutron measurements obtained from the two Luserna stone specimens exceeded the background level by approximately one order of magnitude, when catastrophic failure occurred. The first specimen reached at time T = 32 minutes a peak load of ca 400 kN, corresponding to an average pressure on the bases of 111.1 MPa. When failure occurred, the count rate was found to be $(28.3\pm0.2)\ 10^{-2}$ cps, corresponding to an equivalent flux of thermal neutrons of $(43.6\pm0.3)\ 10^{-4}\ n_{thermal}$ cm^{-2} s^{-1}. The second specimen reached at time T = 29 min a peak load of ca 340 kN, corresponding to an average pressure of 94.4 MPa. When failure occurred, the count rate was found to be $(27.2\pm0.2)\ 10^{-2}$ cps, corresponding to an equivalent flux of thermal neutrons of $(41.9\pm0.3)\ 10^{-4}\ n_{thermal}$ cm^{-2} s^{-1}.

In more recent experiments, cylindrical specimens, with different size and slenderness, were selected. For the specimens of larger dimensions, neutron emissions, detected by He^3, were found to be of about one order of magnitude higher than the natural background level at the time of the catastrophic failure. These emissions fully confirmed the preliminary tests [2]–[5], [27]–[35]. For specimens with sufficiently large size and/or slenderness, a relatively high energy emission is expected, and hence a higher probability of neutron emission at the time of failure. Completely different neutron emission levels were found for different rocks [2]–[5], [27]–[35]. In particular, for granitic rocks, with an iron content amount of $\sim$1.5%, a neutron emission up to one order of magnitude greater than the background level was detected. In the case of basalt and magnetite, where the iron concentration is respectively $\sim$15% and $\sim$72.5%, neutron emissions up to 10^2 times (for basalt) and 10^3 times (for magnetite) the environmental level were measured, whereas for marble, no neutron emissions greater than the background were observed. On the other hand, the results obtained from steel specimens subjected to compression or tension up to the final failure were characterized by neutron emissions up to 2.5 times the background level [2].

Furthermore, during compression tests with cyclic loading, an equivalent neutron dose was found at the end of the test by neutron bubble detectors, about twice higher than the background level [4], [5], [32]. In addition, using an ultrasonic horn suitably joined to the specimen, ultrasonic tests were carried out on Luserna stone producing a continuous vibration at 20 kHz. At the end of the test, an equivalent neutron dose about twice higher than the background level was detected [4], [29].

After these tests, Energy Dispersive X-ray Spectroscopy (EDS) analysis was performed on different sample spots of external or fracture surfaces of the granite specimens used in the fracture experiments, in order to get information about possible changes in their chemical composition. The results for phengite and biotite (minerals with a higher Fe concentration in granite) show that the relative reduction in the iron abundance seems to be counterbalanced by the increase in lighter elements such as Al, Si, and Mg. In the case of phengite (Fig. 1), the distribution of Fe concentrations shows two different values equal to 6.2% and 4.0% for external and fracture surface respectively (Fig. 1a). The measurement precision or percent resolution is equal to 0.1%. Similarly, the Al concentration (Fig. 1b) shows an average value changing from 12.5% (external surface) to 14.5% (fracture surface). The values of the iron decrease (-2.2%, Fig. 1a) and of the Al increase ($+2.0$%, Fig. 2b) are approximately the same, which is really impressive.

In Figures 2a-d the results for Fe, Al, Si, and Mg concentrations of biotite crystalline phase are shown. In this case, the iron decrease is about 3.0%, from 21.2% (external surface) to 18.2% (fracture surface) (Fig. 2a). At the same time, Al content variations show an average increase of about 1.5% (Fig. 2b). In Figures 2c and 2d it is shown that, in the case of biotite, also Si and Mg contents present considerable variations. The mass percentage of Si changes from a mean value of 18.4% (external surface) to a mean value of 19.6% (fracture surface), with an increase of 1.2% (Fig. 2c). Similarly, the mean value of Mg concentration changes from 1.5% (external surface) to 2.2% (fracture surface), with an increase of 0.7% (Fig. 2d). Therefore, the iron decrease (-3.0%) in biotite is counterbalanced by an increase in aluminum ($+1.5$%), silicon ($+1.2$%), and magnesium ($+0.7$%).
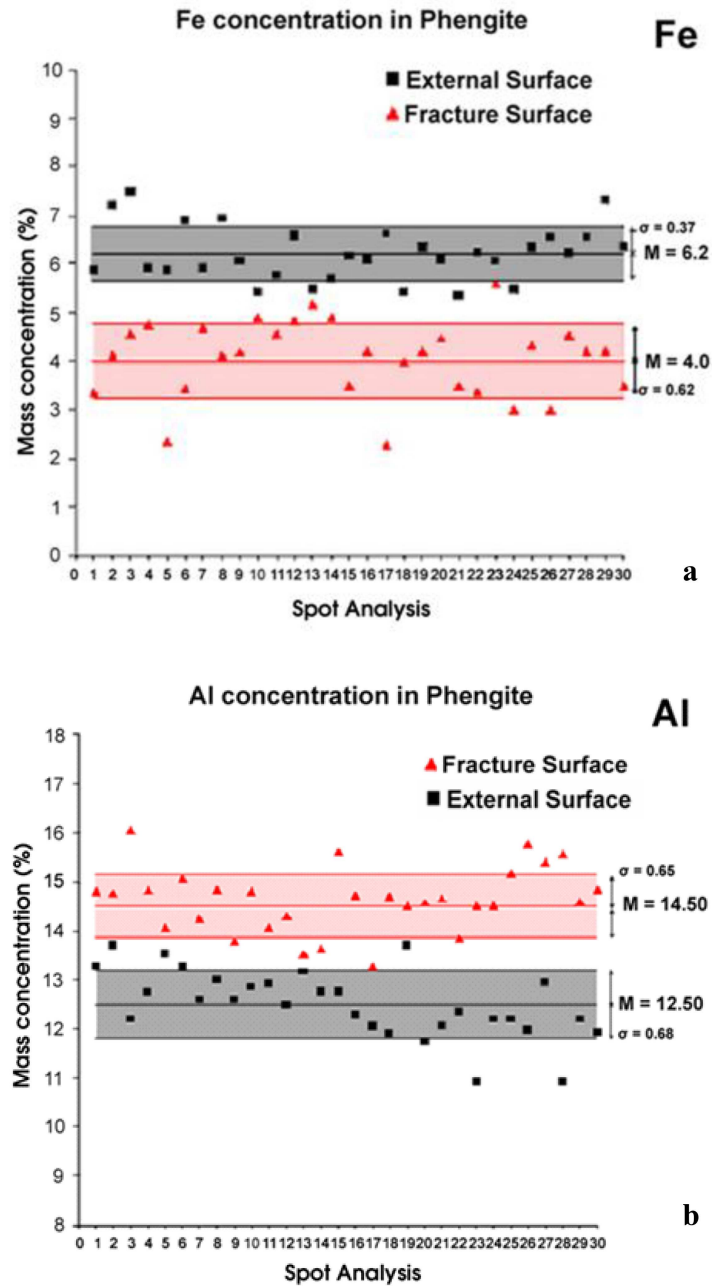
Figure 1. EDS results of Fe and Al concentrations in phengite analysed on samples coming from crushed specimens of granite: (a) Fe concentration on external surfaces (squares) and on fracture surfaces (triangles). The Fe decrease considering the two mean values of the distributions is equal to 2.2%. (b) Al concentration on external surfaces (squares) and on fracture surfaces (triangles). The Al increase, considering the two mean values of the distributions, is equal to 2.0%.
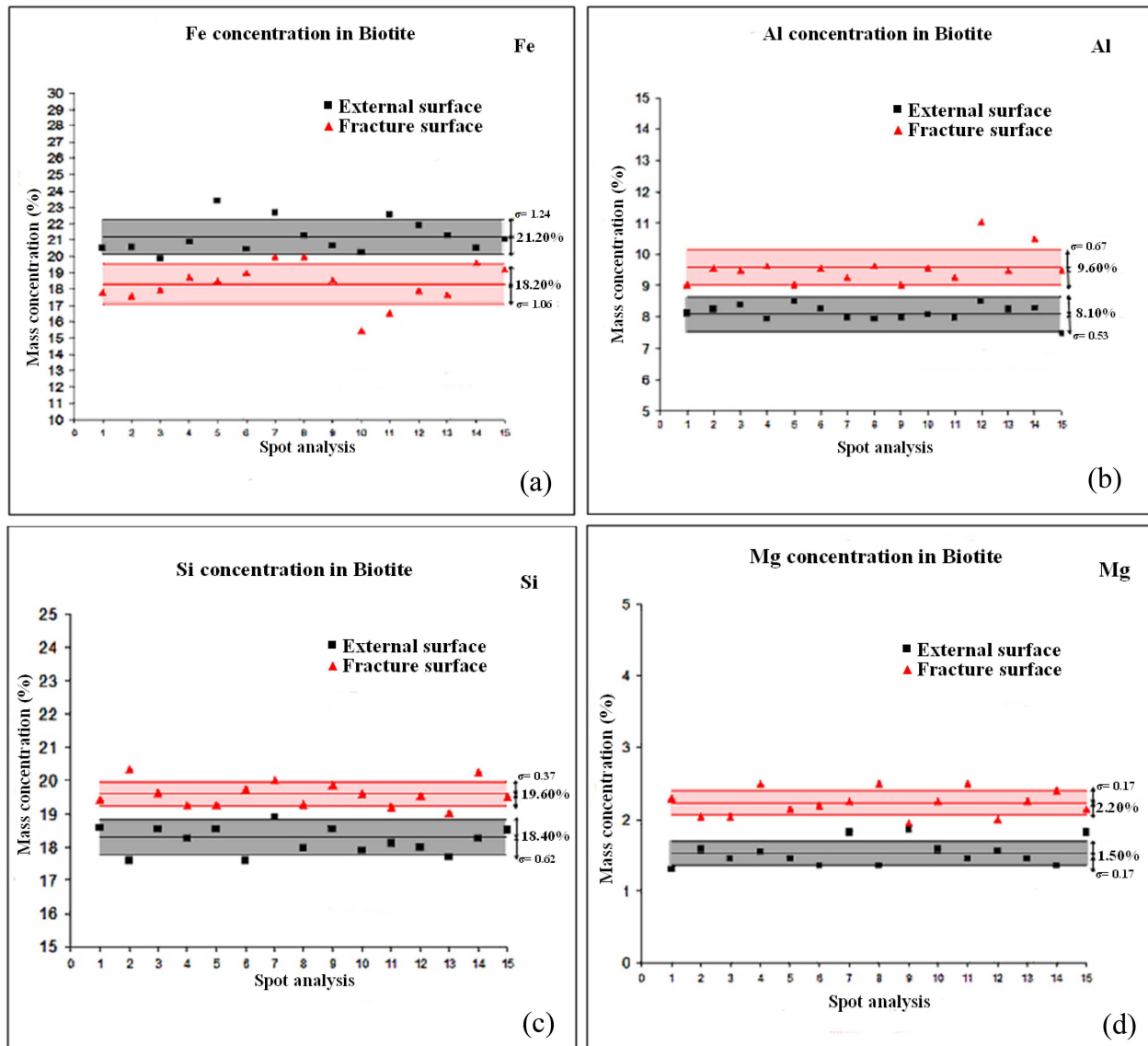
Figure 2. EDS results of Fe (a), Al (b), Si (c), and Mg (d) concentrations in biotite analysed on samples coming from crushed specimens of granite. Considering the analysis done on external and fracture surfaces, the iron decrease (-3.0%) in biotite is counterbalanced by an increase in aluminium ($+1.5\%$), silicon ($+1.2\%$), and magnesium ($+0.7\%$).

4.2. Basalt

After the mechanical loading experiments, Energy Dispersive X-ray Spectroscopy (EDS) was performed on different samples of external and fracture surfaces, belonging to the same specimen used during the cyclic loading test on basalt. The analysis was conducted in order to correlate the neutron emission from the specimen with the variations

in rock composition and to detect possible anomalous transformations from iron to lighter elements. The quantitative elemental analyses were performed by a ZEISS Supra 40 Field Emission Scanning Electron Microscope (FESEM) equipped with an Oxford X-rays microanalysis [5], [32]–[34].

The first analysis was performed on fracture surfaces of a basalt specimen after the fatigue test and the consequent failure. In this case, similarly to the case of Luserna stone [34], taking into account the heterogeneity of the material, the samples were carefully chosen to investigate and compare the same minerals before and after the failure. In particular, olivine was considered due to its high iron content ($\sim$24%) and because it is rather abundant within this type of rock [34].

In Figs. 3a-c, the distributions of Fe, Si, and Mg concentrations in olivine are reported, for external and fracture surfaces. It can be observed that the distribution of Fe content for the external surface shows an average value of 18.4% (Fig 3a). In the same graph, the distribution of Fe concentrations on the fracture sample shows a significant variation. It can be seen that the mean value of the distribution of measurements performed on the fracture surface is equal to 14.4%, considerably lower than the mean value of external surface measurements (18.4%). Similarly to Fig. 3a, in Fig 3b the Si mass percentage concentrations are considered. For Si contents, the observed variations show a mass percentage increase approximately equal to 2.2%. The average value of Si concentration changes from 18.3% on the external surface to 20.5% on the fracture surface. In Fig. 3c it is shown that, in the case of olivine, Mg content also presents considerable variations. Figure 3c shows that the mass percentage concentration of Mg changes from a mean value of 21.2% (external surface) to a mean value of 22.8% (fracture surface) with an increase of 1.6%. Therefore, the iron decrease (-4.0%) in olivine seems to be almost perfectly counterbalanced by an increase in silicon ($+2.2$%) and magnesium ($+1.6$%).

The results reported in Figs. 3 are also important from a geophysical point of view. In fact, at the scale of the Earth's Crust, the non-homogeneous composition of oceanic and continental crusts could be explained by the transition from basaltic to sialic compositions. Comparing the data presented in the literature concerning the composition of the two different types of terrestrial crust, it can be noted that iron concentration changes from $\sim$8%, in the oceanic crust, to $\sim$4% in the continental one [36]–[43].
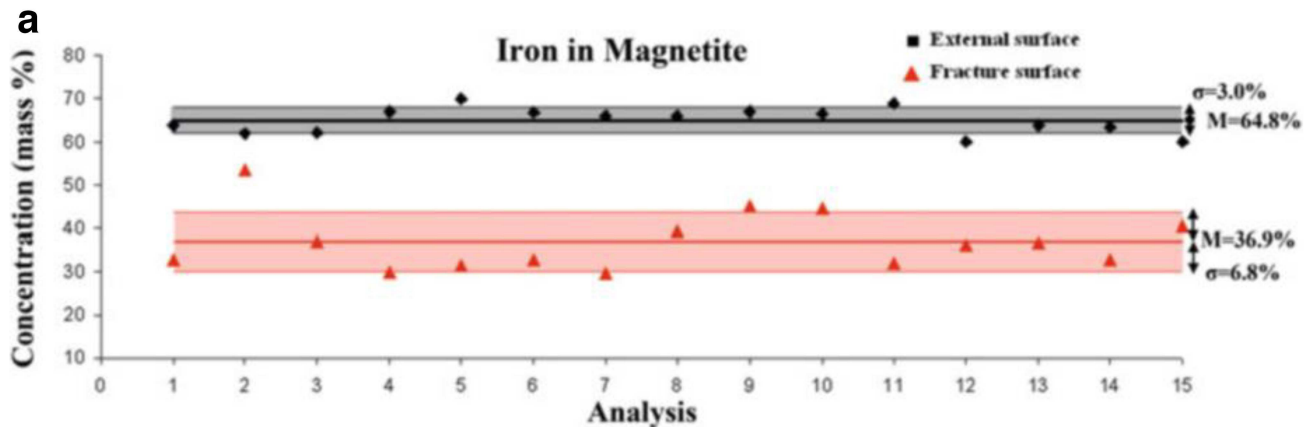
4.3. Magnetite

Similar quantitative results have been obtained also in the case of magnetite. The fracture surfaces of a magnetite specimen were analyzed in order to recognize possible evidence of phono-fission reactions. Taking into account the homogeneity of the chemical composition of this material (Fe-oxides content $\sim$95%), the analysis on the external surface of this rock was conducted in a different manner with respect to granitic and basalt rocks. In this case, in fact, taking into account the homogeneity of the rock, both map and spot analyses were performed to evaluate the composition changes. As mentioned before, the typical composition of magnetite is given by Fe and O, these elements representing about the 95% of this kind of rock. The remaining part is represented by traces of other elements such as Na, Si, Cl, and K. Maps of dimension 250 μm $\times$ 200 μm were analyzed to detect the presence of significant changes in the chemical composition.

In Fig. 4, the chemical element concentrations are reported indicating the mass percentages for both external and fracture surfaces. At a first glance, it can be noted that, for the fracture surface, consistent contents of Al and Mn appear after the specimen failure (Fig. 4), whereas they were absent in the analysis performed on the external surface before the failure test (Fig. 4b,e).

At the same time, on the fracture surface, we observe a significant Fe decrease (Fig. 4a). In order to evaluate these changes from a statistical point of view, 15 analyses on the external surface and 15 on the fracture surface were carried out and reported in Figs 4a-e. In these diagrams, similarly to the results obtained for granite and basalt and reported previously, the mass percentage concentrations for Fe, Al, Si, O, and Mn (Fig. 4) are reported, making a comparison
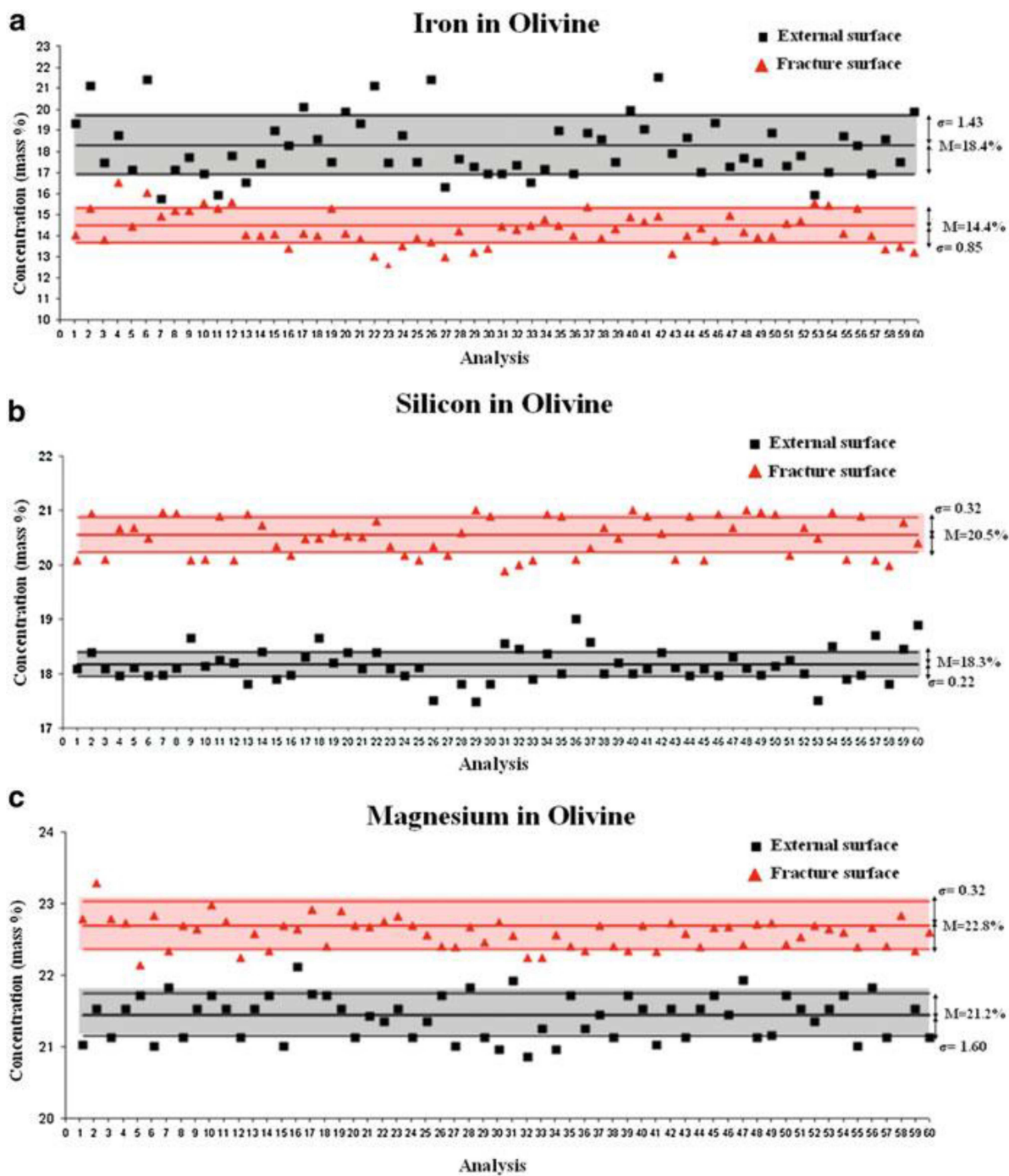
Figure 3. Olivine chemical changes after mechanical loading and crushing: (a) Fe decrease (-4.0%) is almost perfectly counterbalanced by an increase in Si (b) ($+2.2\%$) and Mg (c) ($+1.6\%$).

Figure 4a. Iron chemical element concentration, with mass percentages for both external and fracture surface. Fe decreased by about 27.9% in Magnetite after the brittle fracture of the specimen. The Fe concentration on the external surface was about 64.8% and the concentration on the fracture surface, after the test, was 36.9%.

between external and fracture surfaces. It is interesting to observe a decrease in Fe concentration of 27.9% (from a value of 64.8% down to 36.9%). At the same time, Al concentration increases from zero to a mean value of 10.1%. It is important to consider that approximately one third of the Fe decrease may be counterbalanced by the Al increase. The remaining percent of iron decrease seems to be almost perfectly counterbalanced by the increases in the other elements.

The appearance of Al and Mn, absent before the test, and the almost perfect balance between the Fe decrease (-27.9%) and the increase in the other elements ($+27.7\%$), could be considered as direct evidences that nuclear reactions of a new type take place. Al, Si, O, and Mn are increasing on magnetite fracture surface after the experiments. In particular Al and Mn, with concentrations of about 10.1% and 2.2% after the experiment, were absent before the same experiment, or observable in traces on the external surfaces.

5. Conclusions

Theoretical explanations to these phenomena were recently given by Widom et al [12], [16], in order to justify neutron emissions as a consequence of nuclear reactions taking place in iron-rich rocks during brittle fracture. The same authors argued that neutron emissions may be related to piezoelectric effects and that the iron nucleus splitting may be a consequence of a nuclear photodisintegration.

As a conclusion and according to the experimental results, this hypothesis regarding iron depletion finds very important evidence and confirmation on the scale of the Earth's Crust, when particular pressure waves originate from fracture phenomena as well as before or in correspondence to an earthquake [3]–[5], [27]–[35], [38], [44], [45]. The phono-disintegration reactions are the final conclusions from our theoretical approach, starting from collective oscillations of electronic density inside the solid lattice.

Phono-disintegration reactions can be therefore considered in order to interpret the most significant geophysical and geological transformations, which are still unexplained today. The laboratory results herein reported for granite, basalt, and magnetite give a new and original interpretation to the evolution of the lithosphere of our planet, and contribute to the explanation of the difference between oceanic and continental crust compositions due to subduction and seismic phenomena.
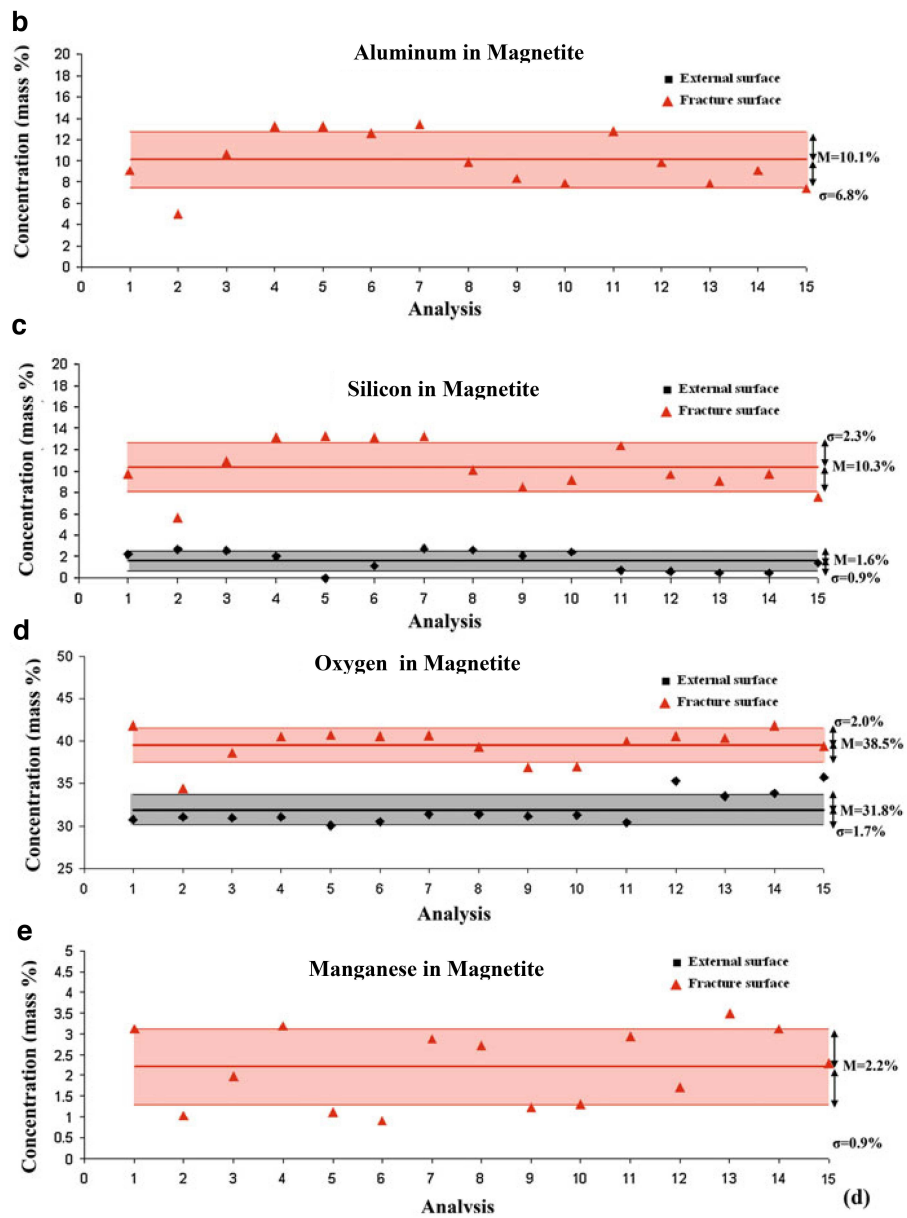
Figure 4b-e. Aluminum, Silicon, Oxygen and Manganese, chemical element concentrations, with mass percentages for both external and fracture surface.

Appendix

Let us consider an electron gas which moves through a lattice dislocation. As a consequence of this electron flow, a charge asymmetry occurs on the opposite sides of the dislocation. As a consequence of the generated opposite sign, a

reactive force appears, generating a simple harmonic motion at the plasmonic frequency, and results in Equation (1) as evaluated in [6]. This relation is difficult to evaluate, so we consider the Relations (3) and (4) into the Equation (1), obtaining:

$$\omega_{ph}^2 = \frac{n_{eff}e^2}{\varepsilon_0 m_{eff}} = \frac{\frac{A}{a^2}ne^2}{\frac{\varepsilon_0\mu_0}{2\pi}ne^2 A \ln\left(\frac{a}{r}\right)} = \frac{2\pi}{\varepsilon_0\mu_0 a^2 \ln\left(\frac{a}{r}\right)} = \frac{2\pi\ c^2}{a^2 \ln\left(\frac{a}{r}\right)} \tag{11}$$

where the plasmonic frequency can be evaluated only in relation to the characteristics of the lattice [1]. Here, the problem is to evaluate the quantity r. Following the results obtained in [6], at first approximation, r can be assumed to be of order of 10^{-6} m. In this way, we are able to evaluate the plasmonic frequency by introducing only one approximation which is the value of r.

Acknowledgments

References

[1] U. Lucia, A. Carpinteri, GeV plasmons and spalling neutrons from crushing of iron rich natural rocks, *Chemical Physics Letters*, **640** (2015), 112–114.

[2] A. Carpinteri, TeraHertz Phonons and Piezonuclear Reactions from Nano-scale Mechanical Instrabilities, in: A. Carpinteri, G. Lacidogna and A. Manuello (Eds.), *Acoustic, Electromagnetic, Neutron Emissions from Fracture and Earthquakes* (Springer International Publishing, Switzerland 2015), pp. 1–10.

[3] F. Cardone, A. Carpinteri, G. Lacidogna, Piezonuclear neutrons from fracturing of inert solids, *Physics Letters A*, **373** (2009), 4158–4163.

[4] A. Carpinteri, O. Borla, G. Lacidogna, A. Manuello, Neutron emissions in brittle rocks during compression tests: Monotonic vs. cyclic loading, *Physical Mesomechanics*, **13** (2010), 268–274.

[5] A. Carpinteri, G. Lacidogna, A. Manuello, O. Borla, Piezonuclear fission reactions from earthquakes and brittle rocks failure: Evidence of neutron emission and nonradioactive product elements, *Experimental Mechanics*, **53** (2013), 345–365.

[6] J.B. Pendry, A.J. Holden, W.J. Stewart and I. Youngs, Extremely Low Frequency Plasmons in Metallic Mesostructures, *Physical Review Letters*, **76** (25) (1996), 4773–4776.

[7] N.W. Ashcroft and N.D. Mermin, *Solid State Physics*, (Harcourt, San Diego 1976), pp. XXII + 826.

[8] C. Kittel, *Introduction to Solid State Physics*, 7th edn, (John Wiley & Sons, New York, 1996), pp. 688.

[9] A.S. Davydov, *Theory of Solids*, (Nauka, Moscow, 1980), pp. 308.

[10] A. Manuello, R. Sandrone, S. Guastella, O. Borla, G. Lacidogna and A. Carpinteri, Neutron Emissions and Compositional Changes at the Compression Failure of Iron-rich Natural Rocks, in *Acoustic, Electromagnetic, Neutron Emissions from Fracture and Earthquakes*, Springer International Publishing Switzerland (2015), pp. 23–37.

[11] A. Carpinteri, N. Pugno, Are scaling laws on strength of solids related to mechanics or to geometry?, *Nature Materials*, **4** (2005), 421–423.

[12] A. Widom, J. Swain and Y.N. Srivastava, Neutron production from the fracture of piezoelectric rocks, *Journal of Physics G: Nuclear and Particle Physics*, **40** (2013), 015006 (8 pp).

[13] U. Lucia, Some considerations on the photofission excitation function, *International Journal of Nuclear Energy Science and Technology*, **6**(2) (2011), 146–152.

[14] U. Lucia, A pn-pair mass evaluation in nuclear photofission, *International Journal of Nuclear Energy Science and Technology*, **4**(3) (2009), 196–200.

[15] G. Kaniadakis, U. Lucia and P. Quarati, Probability and time of photofission in the quasi deuteron energy region, *International Journal of Modern Physics E*, **2**(4) (1993), 827–834.

[16] A. Widom, J. Swain, Y. N. Srivastava, Photo-disintegration of the iron nucleus in fractured magnetite rocks with magnetostriction, *Meccanica*, **50** (2015), 1205–1216.

[17] J.A. VanGordon, B.B. Gall, S.D. Kovaleski, E.A. Baxter, B.H. Kim, J.W. Kwon and G.E. Dale, Electrical analysis of piezoelectric transformers and associated high-voltage output circuits, *Pulsed Power Conference (PPC)*, 2011 IEEE, Chicago, IL, 19–23 June 2011, 475 – 479.

[18] D. Cirillo, R. Germano, V. Tontodonato, A. Widom, Y.N. Srivastava, E. Del Giudice, and G. Vitello, Experimental Evidence of a Neutron Flux Generation in a Plasma Discharge Electrolytic Cell, *Key Engineering Materials*, **495** (2012), 104–107.

[19] A. Annila, The meaning of mass, *International Journal of Theoretical and Mathematical Physics*, **2**(4) (2012), 67–78.

[20] A. Annila, All in action, *Entropy*, **12** (2010), 2333–2358.

[21] A. Annila and S. Salthe, Cultural naturalism, *Entropy*, **12** (2010), 1325–1343.

[22] P. Tuisku, T.K. Pernu and A. Annila, In the light of time, *Proceedings of the Royal Society A. Mathematical, physical and engineering sciences*, **465** (2009), 1173–1198.

[23] A. Alabastri, S. Tuccio, A. Giugni, A. Toma, C. Liberale, G. Das, F. De Angelis, E. Di Fabrizio and R. Proietti Zaccaria, Molding of plasmonic resonances in metallic nanostructures: Dependence of the non-linear electric permittivity on system size and temperature, *Materials*, **6** (2013), 4879–4910.

[24] M. A. Ordal, L. L. Long, R. J. Bell, S. E. Bell, R. R. Bell, R. W. Alexander, and C. A. Ward, Optical properties of the metals Al, Co, Cu, Au, Fe, Pb, Ni, Pd, Pt, Ag, Ti, and W in the infrared and far infrared, *Applied Optics*, **22** (1983), 1099–1119.

[25] V.E. Levin (translated by L.N. Bell), Nuclear physics and nuclear reactors, MIR Publisher, Moscow, 1981.

[26] E. Segre, Nuclei & Particles (2nd ed.), W.A. Benjamin Inc., San Francisco, 1977.

[27] A. Carpinteri, F. Cardone, G. Lacidogna, Piezonuclear neutrons from brittle fracture: Early results of mechanical compression tests, *Strain*, **45** (2009), 332–339.

[28] A. Carpinteri, F. Cardone, G. Lacidogna, Energy emissions from failure phenomena: Mechanical, electromagnetic, nuclear, *Experimental Mechanics*, **50** (2010), 1235–1243.

[29] A. Carpinteri, G. Lacidogna, A. Manuello, O. Borla, Energy emissions from brittle fracture: Neutron measurements and geological evidences of piezonuclear reactions, *Strength, Fracture and Complexity*, **7** (2011), 13–31.

[30] A. Carpinteri, G. Lacidogna, A. Manuello, O. Borla. Piezonuclear transmutations in brittle rocks under mechanical loading: Microchemical analysis and geological confirmations, in: Kounadis A.N., Gdoutos E.E. (Eds.) *Recent Advances in Mechanics* (Springer, Dordrecht 2010), pp. 361–382.

[31] A. Carpinteri, G. Lacidogna, O. Borla, A. Manuello, G. Niccolini, Electromagnetic and neutron emissions from brittle rocks failure: Experimental evidence and geological implications, *Sadhana*, **37** (2012), 59–78.

[32] A. Carpinteri, G. Lacidogna, A. Manuello, O. Borla, Piezonuclear fission reactions: evidences from microchemical analysis, neutron emission, and geological transformation, *Rock Mechanics and Rock Engineering*, **45** (2012), 445–459.

[33] A. Carpinteri, O. Borla, G. Lacidogna, A. Manuello. Piezonuclear reactions produced by brittle fracture: From laboratory to planetary scale. Proceedings of the 19th European Conference of Fracture, Kazan, Russia, 2012.

[34] A. Carpinteri, A. Chiodoni, A. Manuello, R. Sandrone, Compositional and microchemical evidence of piezonuclear fission reactions in rock specimens subjected to compression tests, *Strain*, **47**(2) (2011), 267–281.

[35] A. Carpinteri, O. Borla, Nano-scale fracture phenomena and TeraHertz pressure waves as the fundamental reasons for geochemical evolution, *Strength, Fracture and Complexity*, **11** (2018), 149–168.

[36] J. Verkaeren, P. Bartholomè, Petrology of the San Leone magnetite skarn deposit (S. W. Sardinia), *Economic Geology*, **74** (1979), 53–66.

[37] J.C. Tanguy, Tholeiitic basalt magmatism of Mount Etna and its relations with the alkaline series, Contributions to Mineralogy and Petrology, **66** (1978), 51–67.

[38] A. Carpinteri, A. Manuello, Geomechanical and Geochemical evidence of piezonuclear fission reactions in the Earth's Crust, *Strain*, **47** (2011), 282−292.

[39] C.D. Catling, K.J. Zahnle, The planetary air leak, *Scientific American*, **300** (2009), 24–31.

[40] S.R. Taylor, S.M. McLennan, The geochemical evolution of the continental crust, *Reviews of Geophysics*, **33** (1995), 241–265.

[41] S.R. Taylor, S.M. McLennan. *Planetary Crusts: Their Composition, Origin and Evolution*, Cambridge University Press, Cambridge, 2009.

[42] C.M.R. Fowler. *The Solid Earth: An Introduction to Global Geophysics*, Cambridge University Press, Cambridge, 2005.

[43] R.L. Rudnick, D.M. Fountain, Nature and composition of the continental crust: A lower crustal perspective, *Reviews of Geophysics*, **33** (2005), 267–309.

[44] A. Carpinteri, O. Borla, Fracto-emissions as seismic precursors, *Engineering Fracture Mechanics*, **177** (2017), 239–250.

[45] A. Carpinteri, O. Borla, Acoustic, electromagnetic, and neutron emissions as seismic precursors: The lunar periodicity of low-magnitude seismic swarms, *Engineering Fracture Mechanics*, **210** (2019), 29–41.